

Electronic supplementary information

Naphthalene Diimide As a Two-Electron Anolyte for Aqueous and Neutral pH Redox Flow Batteries

Veerababu Medabalmi,^{1,2} Mahesh Sundararajan,^{1,2} Vikram Singh,^{1,3} Mu-Hyun Baik^{1,2*}
and Hye Ryung Byon^{1,3*}

¹Department of Chemistry, Korea Advanced Institute of Science and Technology (KAIST), 291 Daehak-ro, Yuseong-gu, Daejeon 34141, Republic of Korea

²Center for Catalytic Hydrocarbon Functionalizations, Institute for Basic Science (IBS), Daejeon 34141, Republic of Korea

³Advanced Battery Center, KAIST Institute for NanoCentury, 291 Daehak-ro, Yuseong-gu, Daejeon 34141, Republic of Korea

Experimental

Materials:

1,4,5,8-Naphthalenetetracarboxylic dianhydride (NTCDA) and Glycine were purchased from Alfa Aesar and used without further purification. All other chemicals were obtained from Sigma-Aldrich and used as received.

Syntheses:

Synthesis of title compounds [K₂-BNDI] and [Na₂-BNDI] were carried out in two steps as per reported method (**Scheme 1**) [1]. In the first step 1,4,5,8-naphthalenetetracarboxylic dianhydride (NTCDA) was refluxed with glycine in glacial acetic acid for 4 h to obtain N,N'-bis(glycinylnaphthalene diimide (H₂-BNDI). Next, stoichiometric quantities of H₂-BNDI (2 mM) and K₂CO₃ (2 mM) were added to 40 mL of 1:4 (v/v) ratio of water and absolute ethanol solution. The mixture was stirred at 60 °C for 12 h and the precipitate was washed with ethanol. The product potassium salt of N,N'-bis(glycinylnaphthalene diimide [K₂-BNDI] was dried overnight at 70 °C in the air oven (yield: 92%). The same method was followed to prepare [Na₂-BNDI] from Na₂CO₃ and H₂-BNDI precursors.

¹H and ¹³C NMR analyses of [K₂-BNDI] (**Figure S1**): ¹H NMR (D₂O, 400 MHz): δ 8.54 (s, 4H, Ar-H), δ 4.78 (s, 4H, -CH₂-), ¹³C NMR (D₂O, 400 MHz): δ 174.46 (-COOK), δ 163.45 (-N-C=O), δ 131.00 (Ar-C), δ 125.77 (Ar-C), δ 125.68 (Ar-C), δ 43.77 (-CH₂-). Ar indicates an aromatic group. ¹H and ¹³C NMR spectra were recorded at Bruker AVANCE 400 MHz spectrometer. Chemical shift was expressed in ppm values with tetramethylsilane (TMS) as the external reference.

Cyclic voltammetry (CV) studies:

CV studies were carried out on three-electrode cell consisting 3 mm diameter of a glassy carbon (GC) as the working electrode (WE), platinum wire as the counter electrode (CE) and a leak free Ag/AgCl as the reference electrode. All CV data were converted to the NHE reference by using an internal reference of [Fe(CN)₆]³⁻/[Fe(CN)₆]⁴⁻ (*E*_{red} = 0.358 V vs NHE). CV measurements were conducted using VMP3 (Biologic) electrochemical tester. All CV tests were performed at ambient conditions. The CV curves of [K₂-BNDI] are presented in the **Figure 1** and Randles-Sevcik's plots for the first and second redox events are **Figure S2**. **Figure S5** shows CV curves of [Na₂-BNDI] in the same condition.

Rotating disk electrode (RDE) measurements:

RDE experiments were performed using an ALS RRDE-3A instrument equipped with a 3 mm diameter of disk GC as the WE, a Pt wire as the CE and a leak-free Ag/AgCl as the RE. All measurements were conducted at ambient conditions with rotating disk electrode at the speed range from 100 to 1200 rpm and a potential sweeping at 5 mV/s. All CV data were also converted to the NHE reference by using an internal reference of $[\text{Fe}(\text{CN})_6]^{3-}/[\text{Fe}(\text{CN})_6]^{4-}$ ($E_{red} = 0.358$ V vs NHE). Two limiting current plateaus were observed for successive reductions of $[\text{K}_2\text{-BNDI}]$ (**Figure S3**) and $[\text{Na}_2\text{-BNDI}]$ (**Figure S6**), and the mass-transport controlled limiting currents (i_L) of both redox processes were found to be linearly dependent on the square root of the rotation rates ($\omega^{1/2}$). The diffusion coefficients (D) of reduced forms of $[\text{K}_2\text{-BNDI}]$ and $[\text{Na}_2\text{-BNDI}]$ were calculated by plotting i_L against $\omega^{1/2}$ and using Levich equation (**eq. S1**)

$$i_L = 0.62nAFD^{2/3}\eta^{-1/6}C_0\omega^{1/2} \quad (\text{S1})$$

where i_L is the limiting current (A/cm²), n is the number of electrons transferred during the course of the reaction, F is the Faraday's constant (96485 C/mol), D is the diffusion coefficient (cm²/s), A is the area of the electrode (0.07 cm²), ω is the angular rotation rate of the electrode (rad/s), C_0 is the concentration of the analyte (10 mM $[\text{K}_2\text{-BNDI}]$ or 10 mM $[\text{Na}_2\text{-BNDI}]$) and η is the kinematic viscosity (0.01 cm²/s for both 1 M KCl and 1 M NaCl).

Calculating the electron transfer rate constants:

The electron transfer rate constants (k^0) were calculated by the method of Nicholson [2] using following equations (**eqs. S2–S3, Figure S4**).

$$\Psi = k^0(\pi DnF/RT)^{-1/2}v^{-1/2} \quad (\text{S2})$$

The Ψ value can be obtained by Kingler and Kochi (**eq. S3**) [3]

$$\Psi = (-0.6288 + 0.0021\Delta E_p)/(1 - 0.017\Delta E_p) \quad (\text{S3})$$

where k^0 is the electron rate transfer constant (cm/s), v is the scan rate of the CVs (mV/s), D is the diffusion coefficient estimated from RDE studies and ΔE_p is the potential difference between the oxidation and reduction peaks at various scan rates in CV.

Stability studies of [K₂-BNDI] anolyte using static and symmetric H cell:

A three-electrode type of symmetric and static H-cell cell (**Figure 2**) was assembled in order to examine the chemical and electrochemical stability of [K₂-BNDI]. A 3 mL of 5 mM [K₂-BNDI] was fully reduced to [K₂-BNDI]²⁻ through pre-electrochemical reaction, which was used for the catholyte. The symmetric H cell consisted of 2.5 ml of 5 mM [K₂-BNDI] anolyte and 5 mM [K₂-BNDI]²⁻ catholyte above-mentioned, with 1 M KCl supporting electrolyte in each chamber that was separated by AEM. The carbon felts were placed in both sides of chambers. The one in the anolyte chamber was employed as WE coupled with a leak free Ag/AgCl RE, while another in the catholyte chamber acted as CE. The detailed schematic view was depicted in **Figure 2a**.

Evaluation of RFB cycling performance using flow cells:

A zero-gap flow cell was assembled with two carbon felts (thickness (*t*): 3 mm, ES group, Republic Korea) sandwiched with monovalent anion exchange membrane (AEM, *t*: 110 μm, pore size ~10 Å, Selemion, Neosepta, Japan) (**Figure S7–S12**). Pre-tests using different membranes, such as Daramic and Nafion showed poorer performance than AEM. The active area of the flow cell is 6 cm² determined by the size of carbon felts. Each external electrolyte reservoirs contains 15 mL anolyte solution, such as [K₂-BNDI] or [Na₂-BNDI] for the anolytes and 4-OH-TEMPO for the catholyte with supporting electrolytes (1 M KCl, NaCl or KNO₃, **Figure S8 and S15**). The pH values of all electrolyte solutions are 7.0-7.3. The anolyte and catholyte solutions with continuous purging of argon gas were circulated through carbon felts using a peristaltic pump (SHENCHEN, LabV1, China) at a flow rate of 15 mL/min at 5 and 10 mA/cm². The flow rate increased to 20 mL/min at 15 and 20 mA/cm². The flow cell was galvanostatically cycled at 25 °C and in the voltage window of 0.6 to 1.7 V using VMP3 (Biologic). The volumetric capacity was calculated by taking the volume of anolyte alone. The theoretical capacity was estimated using **eq. S4** below.

$$Capacity (C) = \frac{mnF}{MV} \quad (\text{S4})$$

where *m* is the mass of the active material (g), *n* is the number of electrons, *F* is the Faraday's constant (26.8 Ah), *M* is the molar mass of the active material (g/mol) and *V* is the volume of the catholyte or anolyte (L). For 15 mL of 25 mM [K₂-BNDI] anolyte, the theoretical capacity is estimated to 1.34 Ah/L (**eq. S5**).

$$\frac{(0.172 \times 2 \times 26.8)}{(458.46 \times 0.015)} = 1.34 \text{ Ah/L} \quad (\text{S5})$$

The solubility of BNDI molecules was measured using UV-Vis spectrometry (Lambda 265, PerkinElmer) (**Figure S9**).

***Ex-situ* ¹H NMR and electrospray ionization-mass spectroscopy (ESI-MS) analyses:**

Post-mortem ¹H NMR (Bruker AV400, 400 MHz) of [K₂-BNDI] and [Na₂-BNDI] analyte was carried out after cycling of the flow cells with various current densities (**Figure S11** and **Figure S14**). The analytes were dried under reduced pressure using a rotary evaporator, and prepared ¹H NMR samples by adding D₂O solvent.

ESI-MS (Agilent 6224 TOFLC/MS) with the positive ionization mode was utilized to investigate cycling stability of [Na₂-BNDI] from an aqueous flow cell (**Figure 5c**) and the crossover between [K₂-BNDI] anolyte and 4-OH-TEMPO catholyte through AEM (**Figure S12**). A 3 mL of 10 mM 4-OH TEMPO and 3 mL of 5 mM [K₂-BNDI] in 1 M KCl were added to a static H cell and rested for 3 days at open circuit voltage (OCV) in an argon-filled glove box. Then the analytes were diluted to 1 mM and carried out ESI-MS analysis.

Density functional theory (DFT) calculations:

We have constructed a geometric model of [K₂-BNDI] from the CCDC structural database (CCDC code: BOTCIX).[4] Both geometry optimizations and vibrational frequency computations are carried out using density functional theory (DFT).[5] DFT calculations were carried out as implemented in the ORCA 4.0.1 of *ab initio* quantum chemistry program.[6] Geometry optimizations were performed with BP86 functional [7,8] including Grimme's D3 dispersion correction [9] with Becke-Johnson damping factor (D3BJ).[10] All atoms are represented using def2-TZVP basis set.[11] The calculations are accelerated using a resolution of identity (RI) approximation by incorporating the corresponding auxiliary basis set. Analytical vibrational frequencies within the harmonic approximation were computed with the abovementioned basis sets to confirm proper convergence to well-defined minima. Standard approximation was used to obtain zero-point vibrational energy and entropy corrections. We obtained solvation energies using the optimized gas phase structures from the CPCM solvation model with dielectric constant $\epsilon = 80.4$ (water) using the default radii as implemented in ORCA. Chimera 1.12c [12] is used to plot to plot the molecular orbitals (iso value of 0.05).

Redox potentials w.r.t NHE are calculated using the following equation,

$$1^{\text{st}} \text{ redox potential } \Delta G_{\text{soln}} = \Delta G_{\text{soln}}([\text{K}_2\text{-BNDI}]^- - [\text{K}_2\text{-BNDI}])$$

$$2^{\text{nd}} \text{ redox potential } \Delta G_{\text{soln}} = \Delta G_{\text{soln}}([\text{K}_3\text{-BNDI}]^{+} + (\text{H}_2\text{O})_8 - [\text{K}_2\text{-BNDI}]^- - [\text{K}(\text{H}_2\text{O})_8]^{+})$$

$$E^{\circ} = -\Delta G_{\text{soln}} - 4.28$$

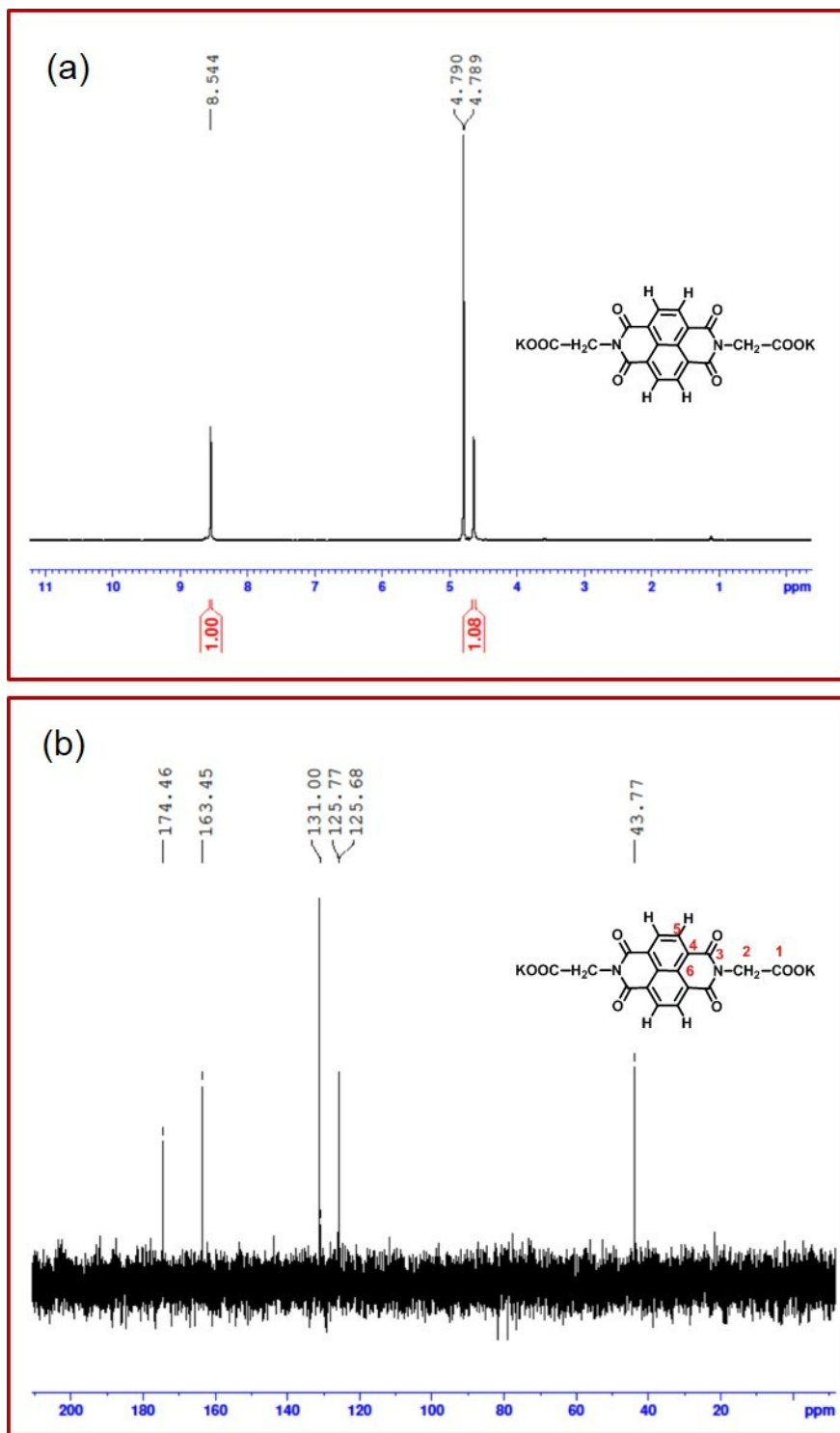


Figure S1. (a) ^1H NMR and (b) ^{13}C NMR spectra of [K₂-BNDI] in D₂O solvent at room temperature.

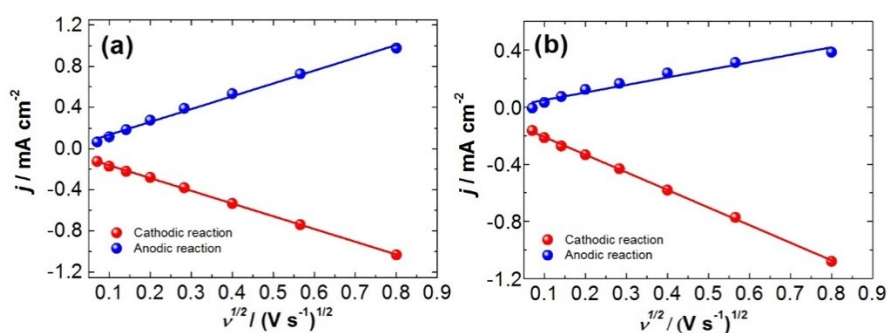


Figure S2. Randles-Sevcik (R-S) plots of peak current density (j) versus square root of the scan rate ($v^{1/2}$) for (a) the first redox event of $[K_2\text{-BNDI}]/[K_2\text{-BNDI}]^{1-}$ and (b) the second redox couple of $[K_2\text{-BNDI}]^{1-}/[K_2\text{-BNDI}]^{2-}$. The data were obtained from CV curves of 5 mM $[K_2\text{-BNDI}]$ in 1 M KCl (aq) at scan rates starting from 5 to 640 mV/s at ambient conditions (**Figure 1b**).

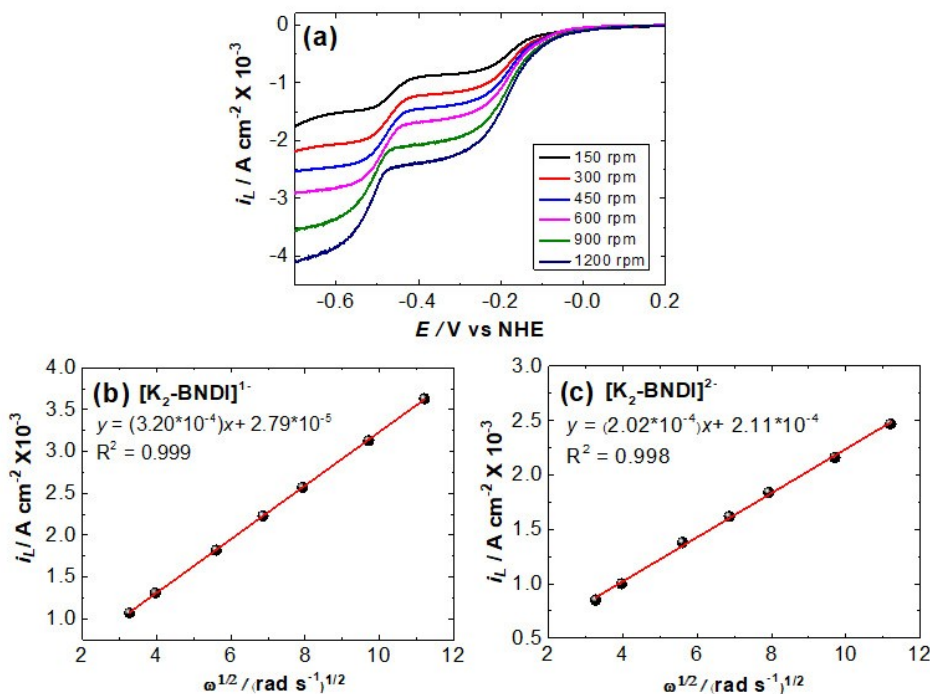


Figure S3. RDE tests and the corresponding Levich plot for 10 mM $[K_2\text{-BNDI}]$ in 1 M KCl(aq) at ambient conditions. (a) Linear sweep voltammetry (LSV) at a potential sweeping of 5 mV/s with rotating of disk GC electrode in various speeds from 100 to 1200 rpm. (b–c) Corresponding Levich plots for (b) the first and (c) the second electrochemical reduction of $[K_2\text{-BNDI}]$. The calculated D values are 3.95×10^{-6} and 1.95×10^{-6} cm^2/s for the first and second reduction of $[K_2\text{-BNDI}]$ respectively.

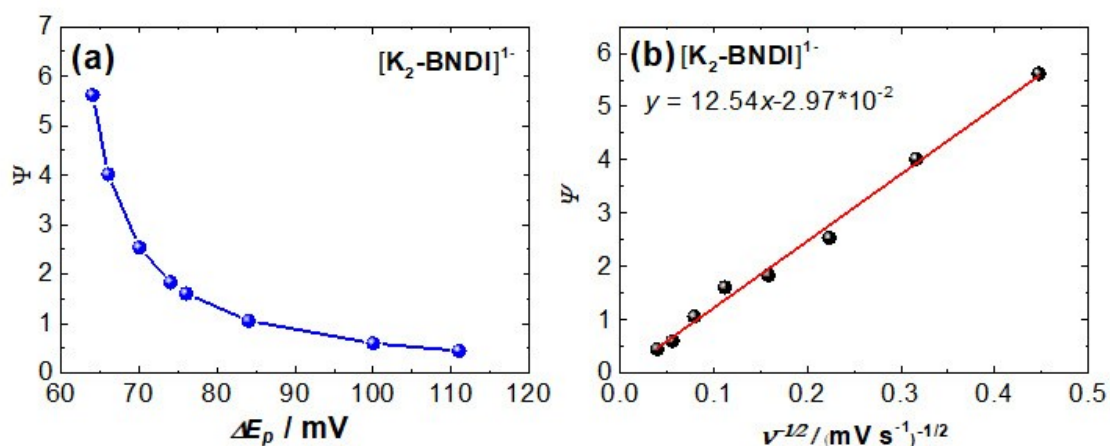


Figure S4. Estimation of rate constants (k^0) of $[K_2-BNDI]$ by the method of Nicolson. (a) Plots of Ψ vs. ΔE_p for the first redox process of $[K_2-BNDI]$. ΔE_p is estimated from CV studies of 5 mM $[K_2-BNDI]$ in 1 M KCl at different scan rates starting from 5~640 mV/s. (b) Linear relationship between Ψ and $v^{-1/2}$ of the first redox reaction of $[K_2-BNDI]$. The k^0 calculated by the slope of Ψ against $v^{-1/2}$ is 0.27 cm/s. It should be noted that the reduction potential of the 2nd wave changed notably with increasing the scan rates. This unique behavior of the 2nd reduction, possibly attributable to the ion-pair formation, introduces an uncertain amount of kinetic inhibition and renders the Nicolson method inappropriate.

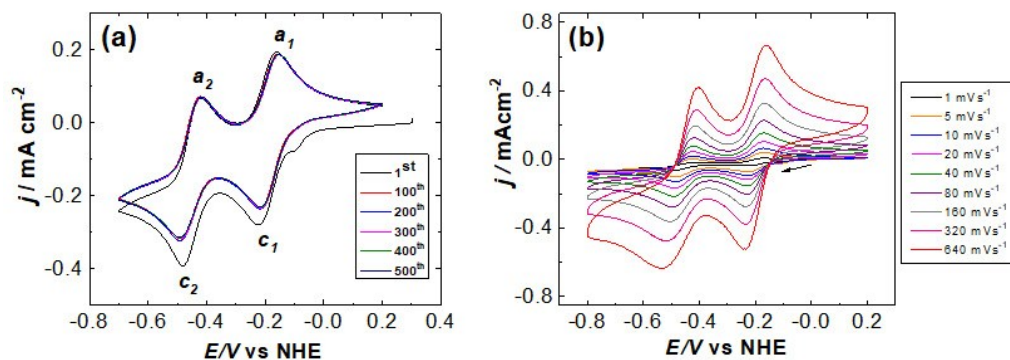


Figure S5. CV curves of $[\text{Na}_2\text{-BNDI}]$ in 1 M NaCl (aq) at ambient conditions with WE: GC, CE: Pt wire and RE: Ag/AgCl. (a) 500-times CV cycle with 5 mM $[\text{Na}_2\text{-BNDI}]$ at a scan rate of 20 mV/s. (b) Potential sweeping curves in the range of 1~640 mV/s with 3mM $[\text{Na}_2\text{-BNDI}]$. The c_1/a_1 indicates $[\text{Na}_2\text{-BNDI}]/[\text{Na}_2\text{-BNDI}]^{1-}$ and the c_2/a_2 denotes $[\text{Na}_2\text{-BNDI}]^{1-}/[\text{Na}_2\text{-BNDI}]^{2-}$. The formal potentials (E^0) are -0.20 and -0.47 V vs. NHE, respectively.

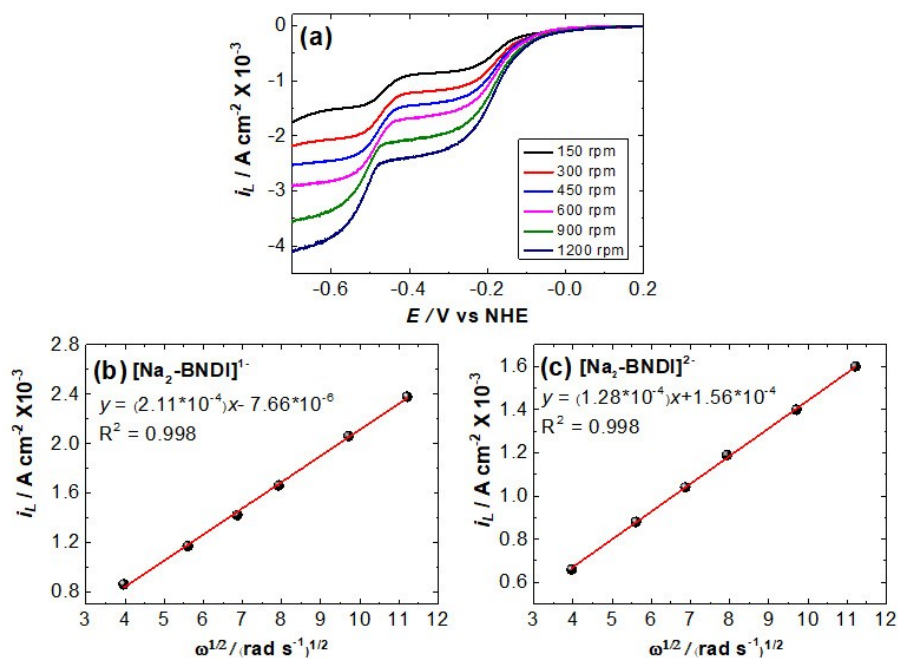


Figure S6. RDE tests and the corresponding Levich plot for 10 mM $[\text{Na}_2\text{-BNDI}]$ in 1 M NaCl(aq) at ambient conditions. (a) LSV at a potential sweeping of 5 mV/s with rotating of disk GC electrode in various speeds from 150 to 1200 rpm. (b–c) Corresponding Levich plots for (b) the first and (c) the second electrochemical reduction of $[\text{Na}_2\text{-BNDI}]$. The calculated D values are 2.13×10^{-6} and 1.01×10^{-6} cm^2/s for the first and second reduction of $[\text{Na}_2\text{-BNDI}]$ respectively.

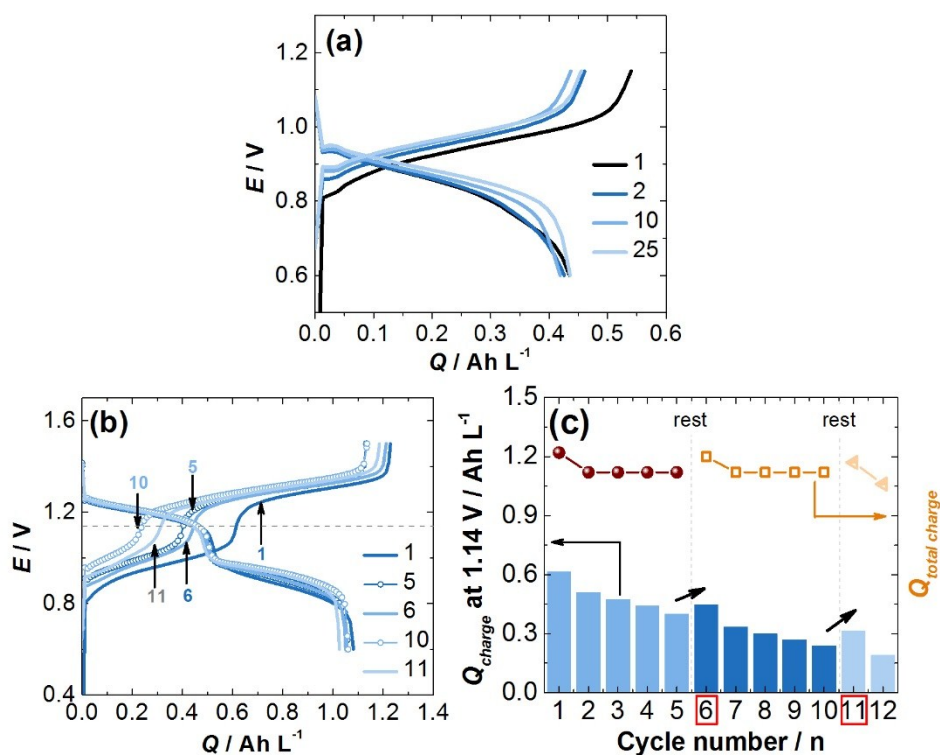


Figure S7. Stability test with aqueous flow cells with 25 mM $[\text{K}_2\text{-BNDI}]||100$ mM 4-OH-TEMPO in 1 M KCl. The flow rate was 15 mL/min for the current density of 5 mA/cm². (a) 25 times galvanostatic cycling at the limited potential for the first redox reaction. In comparison with **Figure 3c** showing the stepwise redox process, the capacity fading and potential shift are not detected. (b-c) Galvanostatic cycling with the resting for 1 day intervened every after 5 cycle. (b) Charge-discharge profiles for 1, 5, 6, 10, and 11th cycle. The dashed line indicated 1.14 V of charge process, at which the first reduction of $[\text{K}_2\text{-BNDI}]/[\text{K}_2\text{-BNDI}]^{1-}$ terminates. (c) Corresponding bar graphs for the charging capacity at 1.14 V, i.e. at the end of the first reduction compared with total charging capacity. The dashed lines indicate the rest for 24 h. The increasing capacities after 1 day rest are apparent.

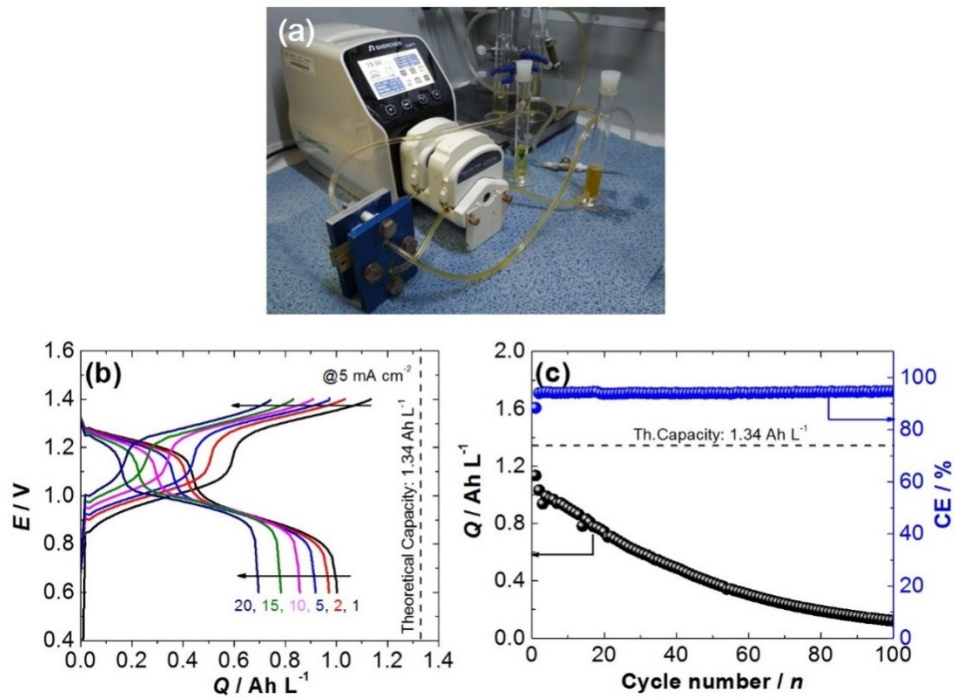


Figure S8. Galvanostatic cycling tests of a flow cell with 25 mM [K₂-BNDI]||50 mM 4-OH-TEMPO in 1 M KCl aqueous solution. The flow rate was 15 mL/min and the current density was 5 mA/cm. (a) Digital photo of a flow cell. (b) Initial 20 cycles of charge-discharge profiles. The dashed line denotes a theoretical capacity, 1.34 Ah/L. (c) Corresponding capacity retention (Q) and Coulombic Efficiency (CE) for total 100 cycles. The flow cell delivered the first capacity of 1.13 Ah/L against the theoretical capacity 1.34 Ah/L. Upon cycling, the cell capacity was gradually decreased and retained only 0.12 Ah/L after 100 cycles.

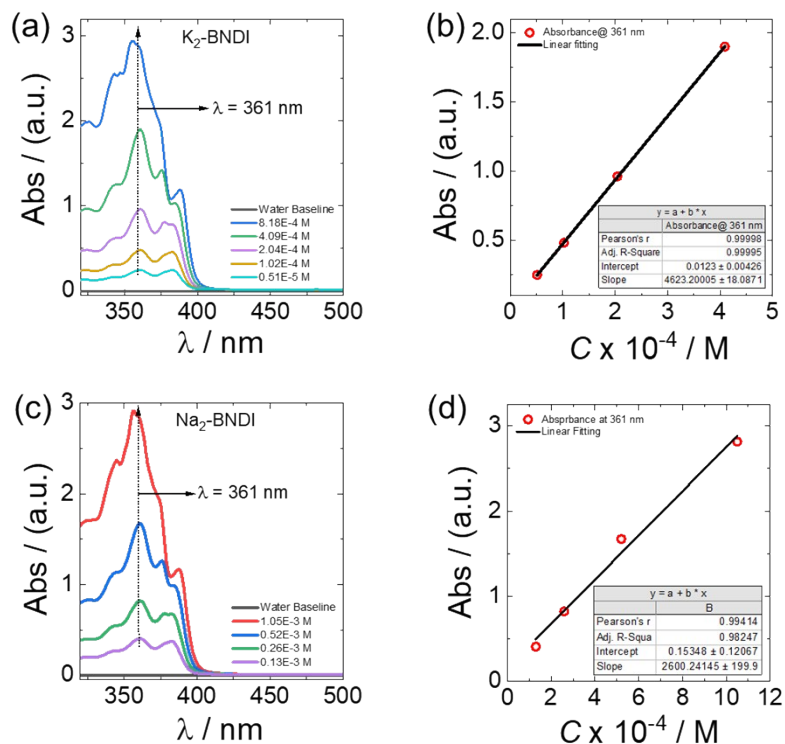


Figure S9. Solubility tests. (a, c) UV-Vis spectra of (a) [K₂-BNDI] and (c) [Na₂-BNDI] with different concentrations without electrolyte salt. (b, d) Corresponding calibration curve for UV-Vis absorbance ($\lambda = 361$ nm) as a function of molecular concentration. The measured maximal solubility of [K₂-BNDI] in DI water was 167 mM, and the [Na₂-BNDI] was 210 mM. After including the electrolyte salt, the maximum solubility of [K₂-BNDI] with 1 M KCl solution was decreased to 30 mM, and [Na₂-BNDI] with 1 M NaCl solution was 41 mM.

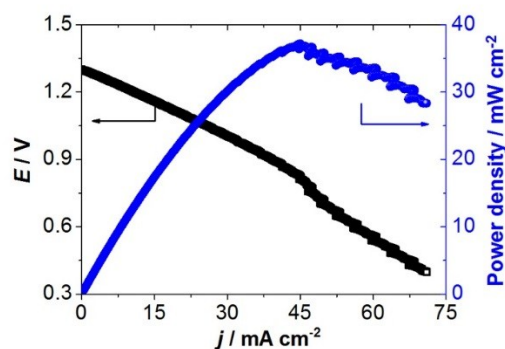


Figure S10. Polarization curve acquired at 100% state of charge (SOC) from LSV at a scan rate of 25 mV/s from an aqueous flow cell with 25 mM [K₂-BNDI]||100 mM 4-OH-TEMPO in 1 M KCl. The flow rate was 15 mL/min. The power density of ~ 37 mW cm^{-2} was calculated to the voltage (V) multiplied by the current density (mA/cm^2).

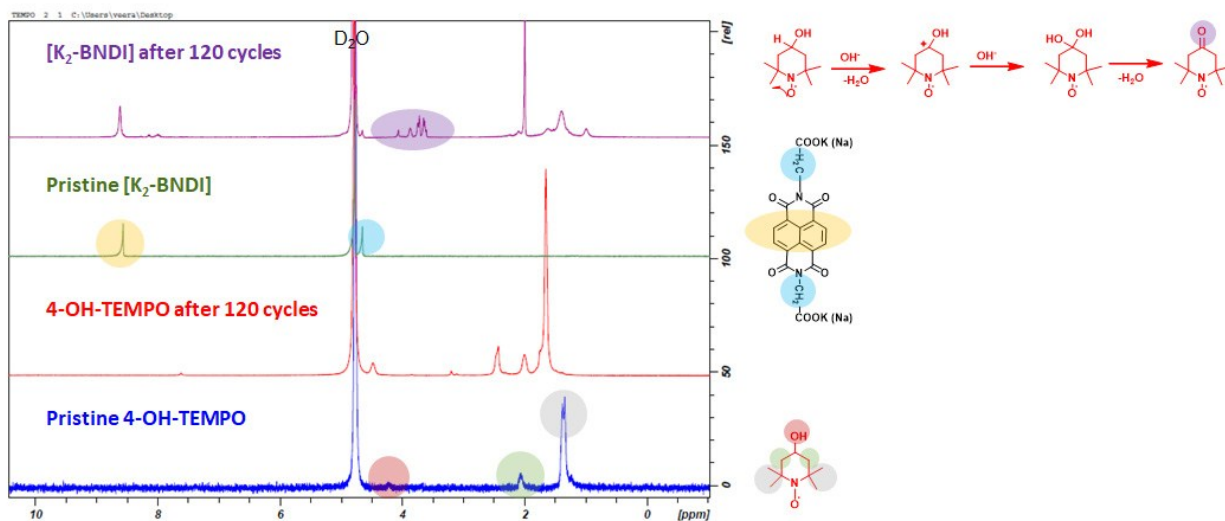


Figure S11. ^1H NMR of $[\text{K}_2\text{-BNDI}]$ and 4-OH-TEMPO before and after 120 cycles in an aqueous flow cell and the corresponding molecular structures. The proton signals from pristine $[\text{K}_2\text{-BNDI}]$ (yellow and blue circles) are detected from anolyte after 120 cycles while the ones from pristine 4-OH-TEMPO (grey, green and red) disappear from catholyte. The various signals appearing for both catholyte and anolyte after cycling may be attributed to the fragments of 4-OH-TEMPO that severely decomposed.

Crossover of 4-OH-TEMPO is very common during the cycling of RFBs. The ^1H NMR graphs revealed that the cycled $[\text{K}_2\text{-BNDI}]$ in the anolyte side contained decomposed 4-OH-TEMPO and minor amounts of 4-OH-TEMPO. The peaks at $\sim 3.5\text{-}4.1$ ppm and 1.8 ppm for $[\text{K}_2\text{-BNDI}]$ after 120 cycles (i.e. the anolyte side) correspond to $-\text{CH}_2$ adjacent to $-\text{C}=\text{O}$, [13] and $-\text{CH}_3$ groups on the piperidine ring, respectively. The intense peak around 1.4 ppm matches well with the peak of $-\text{CH}_3$ group in pristine 4-OH-TEMPO. Other peaks around 0.7 and 1.6 ppm could be due to some fragments formed during the cycling of the cell. These decomposition products are difficult to identify precisely. It should be noted that the decomposition products of 4-OH-TEMPO in the anolyte side are different from the ones in the catholyte side (i.e., 4-OH-TEMPO after 120 cycles) due to different operating potential ranges.

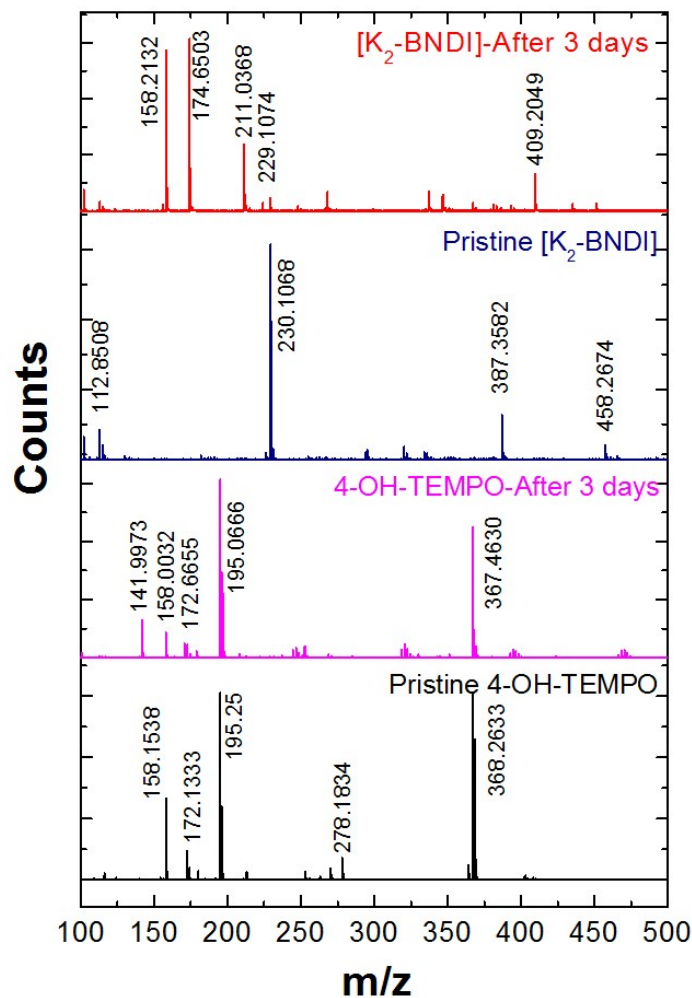


Figure S12. ESI-MS analysis with the positive ionization mode of [K₂-BNDI] (m/z: 458) and 4-OH-TEMPO (m/z: 172) solutions before and after 3 days resting at OCV in the static H cell. The molar concentrations were 25 and 100 mM for [K₂-BNDI] and 4-OH-TEMPO, respectively, which were used for all RFB tests. The fragments of 4-OH-TEMPO detected in the range of 150~250 m/z are observed for both anolyte and catholyte after 3 days, indicating the crossover of 4-OH-TEMPO to anolyte of [K₂-BNDI] side takes place through AEM. The signals related to [K₂-BNDI] are not clearly visible after OCV test, caused by the relatively intense signals from 4-OH-TEMPO.

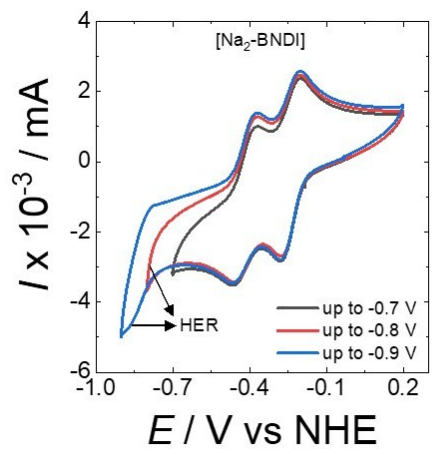


Figure S13. CV graphs of $[\text{Na}_2\text{-BNDI}]$ with 3 mM NaCl at a scan rate of 30 mV/s. The hydrogen evolution reaction (HER) wave was observed below -0.7 V vs. NHE.

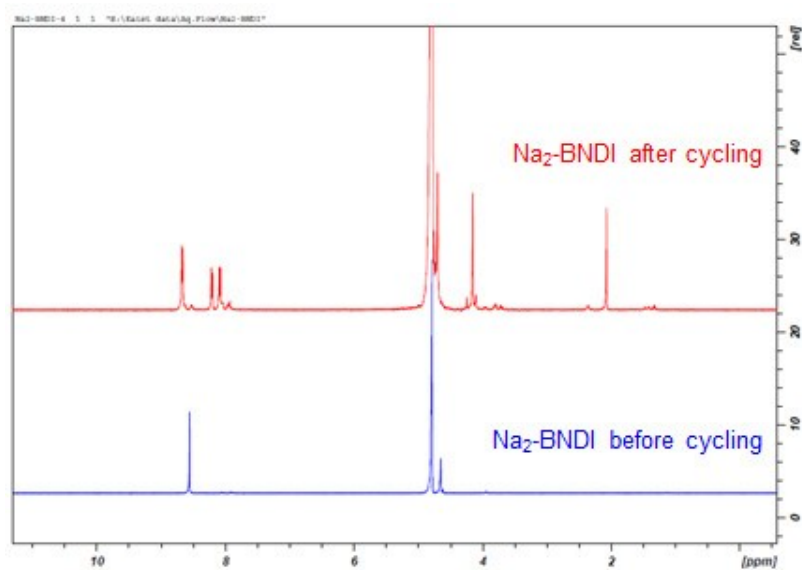


Figure S14. ^1H NMR of $[\text{Na}_2\text{-BNDI}]$ and 4-OH-TEMPO before (blue) and after 200 cycles (red) in an aqueous flow cell. The various signals appearing after cycling may be attributed to the fragments of 4-OH-TEMPO.

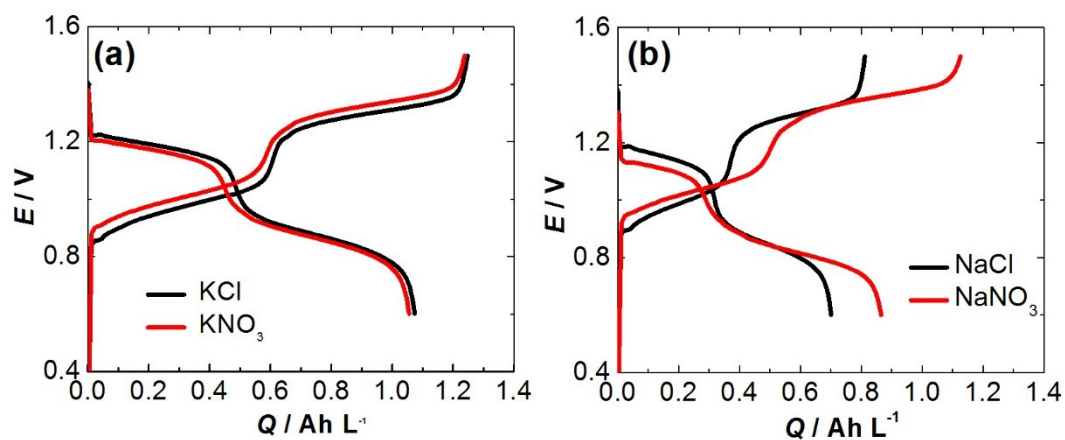


Figure S15. Anion effect of supporting electrolyte by comparing 1 M Cl^- to NO_3^- . (a-b) Galvanostatic charge-discharge profiles for the first cycle from aqueous flow cells with (a) 25 mM $[\text{K}_2\text{-BNDI}]$ or (b) 25 mM $[\text{Na}_2\text{-BNDI}]$ with 100 mM 4-OH-TEMPO. The current density was 5 mA/cm² and a flow rate was 15 mL/min. Larger potential polarizations are measured for NO_3^- in comparison with Cl^- for both $[\text{K}_2\text{-BNDI}]$ and $[\text{Na}_2\text{-BNDI}]$ cells.

Table S1. Summary of the diffusion coefficient (D) and the electron-transfer kinetics (k^0)

		Diffusion coefficient (unit: cm²/s)	Electron-transfer kinetics (unit: cm/s)
[K₂-BNDI]	1 st reduction	3.95×10^{-6}	0.27
	2 nd reduction	1.95×10^{-6}	-
[Na₂-BNDI]	1 st reduction	2.13×10^{-6}	0.20
	2 nd reduction	1.01×10^{-6}	0.12

Table S2. Summary of the calculated and experimental redox potentials.

Equation	Redox potential (vs. NHE)	
	Calculated	Experimental
$[\text{K}_2\text{-BNDI}] + \text{e}^- \rightarrow [\text{K}_2\text{-BNDI}]^-$	-0.196V	-0.20V
$[\text{K}_2\text{-BNDI}]^- + \text{e}^- \rightarrow [\text{K}_2\text{-BNDI}]^{2-}$	-0.785V	
$[\text{K}_2\text{-BNDI}]^- + \text{e}^- + \text{K}^+ \rightarrow [\text{K}_3\text{-BNDI}]^-$	-0.792V	-0.49V
$[\text{K}_2\text{-BNDI}]^- + \text{e}^- + [\text{K}(\text{H}_2\text{O})_8]^+ \rightarrow [\text{K}_3\text{-BNDI}]^- + (\text{H}_2\text{O})_8$	-0.438V	

Optimized coordinates

[K₂-BNDI]

6	2.793258313	-0.339417561	13.504300850
6	3.730338762	0.315924479	14.449785091
6	4.073703938	-0.319047756	15.636891160
1	3.643070850	-1.298366576	15.844089821
6	4.957713455	0.291827015	16.542382217
1	5.235273139	-0.203525822	17.472355743
6	5.501483123	1.541460936	16.269852491
6	6.413586047	2.188203443	17.242096721
6	6.651247565	4.127625455	15.706566799
6	5.713895726	3.472470519	14.761241289
6	5.370555975	4.107555154	13.574180557
1	5.801130639	5.086914975	13.367078673
6	4.486746006	3.496572163	12.668567459
1	4.209215953	3.992066497	11.738648218
6	3.943095264	2.246830015	12.940907719
6	3.031381698	1.599874324	11.968634963
6	4.275045415	1.584615605	14.146461746
6	5.169346913	2.203662557	15.064386783
7	2.488878813	0.367926523	12.320350773
7	6.956816373	3.419741322	16.889984719
6	7.773732423	4.095446010	17.903210573
1	8.647159885	3.476913906	18.138482179
1	8.101837766	5.045412278	17.469235862
6	1.676920995	-0.309955435	11.304405696
1	1.347584724	-1.259438798	11.738469796
1	0.804453381	0.307858539	11.063927164
8	2.296821939	-1.434793423	13.732966727
8	2.756416782	2.135452045	10.885743947
8	7.147373159	5.223152931	15.477953504
8	6.687984013	1.652494824	18.324941566
6	6.968654218	4.330830194	19.210656680
8	5.709013100	4.379339365	19.115948383
8	7.655534409	4.344005145	20.270981245
6	2.489767265	-0.545898403	10.001570280
8	1.809670144	-0.559918462	8.936996063
8	3.748909577	-0.592629953	10.103926112
19	5.951732107	2.493065448	20.891652393
19	3.512114756	1.295619068	8.329046300

[K₂-BNDI]⁻

6	2.826600278	-0.353283746	13.513512760
6	3.737478359	0.304350099	14.446529328
6	4.081135753	-0.330834064	15.658530283
1	3.651493823	-1.312421105	15.857678293
6	4.942863189	0.278181543	16.556210801
1	5.223630956	-0.209689810	17.489793741
6	5.494647721	1.548491551	16.281796413
6	6.378657643	2.190558115	17.238233443
6	6.622221656	4.140729244	15.697589200
6	5.711410385	3.483055253	14.764535654

6	5.367793349	4.118216582	13.552511819
1	5.797435963	5.099803463	13.353364562
6	4.506098989	3.509182128	12.654813068
1	4.225375292	3.997027169	11.721203194
6	3.954292998	2.238884995	12.929241169
6	3.070383351	1.596762840	11.972750110
6	4.279178664	1.577628740	14.141612367
6	5.169714878	2.209774591	15.069451965
7	2.548323539	0.348662246	12.311213986
7	6.900675666	3.438681929	16.899787050
6	7.747652674	4.100543549	17.895245304
1	8.629813144	3.480593120	18.097106169
1	8.057652017	5.051599285	17.445781925
6	1.701436385	-0.313256892	11.315711781
1	1.391550322	-1.264369046	11.765133384
1	0.819193065	0.306588502	11.113882579
8	2.302471687	-1.454333043	13.729955721
8	2.774048768	2.120379735	10.867073672
8	7.146581567	5.241641117	15.481013155
8	6.675157789	1.666844662	18.343822703
6	7.013541310	4.348760590	19.237687106
8	5.763478340	4.542276974	19.197266597
8	7.720137054	4.238437522	20.286021094
6	2.435562436	-0.561311507	9.973255504
8	1.728958256	-0.450981320	8.924931229
8	3.685642996	-0.754741940	10.013653531
19	5.855571838	2.416888640	20.672801982
19	3.593602510	1.370546833	8.538175622

$[K_2\text{-BNDI}]^2\text{-}$

6	2.844503056	-0.359904756	13.517248800
6	3.732812742	0.298908363	14.442580581
6	4.072054703	-0.338509620	15.678342321
1	3.633810086	-1.318594129	15.871862097
6	4.925139066	0.261112811	16.568503224
1	5.209796308	-0.226058009	17.503023475
6	5.494902844	1.545963491	16.290920407
6	6.369822539	2.173617443	17.227469090
6	6.604490377	4.147285464	15.693752282
6	5.716189291	3.488468073	14.768415711
6	5.376952853	4.125882382	13.532650512
1	5.815200240	5.105965466	13.339129495
6	4.523868996	3.526259472	12.642489360
1	4.239214062	4.013428078	11.707967239
6	3.954100487	2.241411776	12.920075161
6	3.079188191	1.613753218	11.983522046
6	4.277750967	1.5744449476	14.137359844
6	5.171249604	2.212927666	15.073637453
7	2.583301745	0.344156076	12.306395543
7	6.865707272	3.443215589	16.904596901
6	7.721737645	4.099562151	17.890917895
1	8.610847684	3.484040754	18.082914261
1	8.018216141	5.050310116	17.425048868
6	1.727289240	-0.312199706	11.320065945
1	1.430791147	-1.262937439	11.785943568
1	0.838189735	0.303326380	11.128037620

8	2.301932884	-1.473806016	13.716121239
8	2.737761671	2.140023483	10.867283549
8	7.147091642	5.261168889	15.494863026
8	6.711261117	1.647342255	18.343701663
6	7.035440412	4.366438479	19.252803359
8	5.794751547	4.627539626	19.259073480
8	7.760296347	4.216786679	20.290632117
6	2.413616890	-0.579106490	9.958200964
8	1.688783213	-0.429478569	8.920353630
8	3.654306912	-0.840202879	9.951964326
19	5.807780795	2.379434724	20.531432909
19	3.641314160	1.407887779	8.679578297

[K₃-BNDI]⁻

6	2.870563814	-0.174961928	13.709068441
6	3.950690847	0.359090799	14.515927293
6	4.316589691	-0.299790263	15.725642932
1	3.789556237	-1.222407667	15.971499757
6	5.296976174	0.211649738	16.539640154
1	5.603788510	-0.295952593	17.455714406
6	5.971464200	1.427665798	16.186111100
6	6.836458103	2.072968579	17.126921603
6	7.137228846	3.979949557	15.537107245
6	6.300062875	3.302049943	14.596740180
6	5.938952936	3.951188265	13.361225905
1	6.482711166	4.854924357	13.080954870
6	4.953117620	3.425208127	12.562952440
1	4.663795285	3.906500097	11.627480708
6	4.267408392	2.226399352	12.923333883
6	3.220606831	1.708736506	12.091081248
6	4.625727222	1.538838643	14.118912494
6	5.661666621	2.078726124	14.961501225
7	2.574222461	0.541944814	12.517902265
7	7.357665655	3.329567474	16.771002937
6	7.800649749	4.159511580	17.891612658
1	8.529297341	3.617270663	18.500525112
1	8.245400724	5.064208806	17.458852034
6	1.514670239	0.010454321	11.659561576
1	1.129975978	-0.877821707	12.177415411
1	0.715192019	0.755365248	11.555753983
8	2.206338607	-1.182999543	14.014180855
8	2.858545417	2.256822558	11.003775389
8	7.532399221	5.182436489	15.387519837
8	7.053500313	1.639356679	18.304143366
6	6.589040739	4.532531044	18.794569238
8	5.457724580	4.704607380	18.201191907
8	6.755426302	4.546513074	20.036555340
6	1.999394549	-0.362353838	10.238110527
8	1.178089194	-0.140758993	9.293199471
8	3.192424936	-0.764220387	10.103222272
19	5.006170467	2.417264588	19.585918330
19	3.240723590	1.367942204	8.647286968
19	4.905229524	5.550476478	15.842431259

[K(H ₂ O) ₈] ⁺			
19	0.000135748	0.000008459	-0.000034315
8	-0.618855147	1.781005018	2.292154781
1	-0.992101115	2.601012181	2.652594911
1	-1.238927718	1.037035419	2.522362359
8	1.781106262	0.618954742	2.292190633
1	2.600856664	0.992674824	2.652727559
1	1.036530294	1.237982954	2.523232837
8	-1.780790639	0.619060483	-2.292238130
1	-1.037170767	1.239748107	-2.521920422
1	-2.600935785	0.992031706	-2.652648149
8	-0.618881514	-1.780971728	-2.292212964
1	-1.239296014	-1.037196552	-2.522139249
1	-0.991981906	-2.601057234	-2.652624626
8	1.781110511	-0.618975096	-2.292231094
1	2.600897888	-0.992636985	-2.652743867
1	1.036625261	-1.238164149	-2.523141792
8	0.619102242	-1.780938573	2.292194334
1	1.238313476	-1.036468070	2.523079952
1	0.992733263	-2.600731868	2.652726692
8	0.619164538	1.780917268	-2.292261369
1	1.238435754	1.036473840	-2.523078847
1	0.992786636	2.600716755	-2.652789356
8	-1.780848950	-0.618996877	2.292154444
1	-2.600936021	-0.992085221	2.652575836
1	-1.037072963	-1.239399402	2.522089842

[H ₂ O] ₈			
8	1.405625934	-1.404564265	1.299470609
8	-1.401986049	-1.402643135	-1.297599322
8	1.408933365	1.409128684	-1.302122017
8	-1.404701496	1.405822444	1.299174160
1	1.475936879	-1.475912913	0.276102014
1	-1.475448585	-1.475303238	-0.274290035
1	1.477633530	1.477773671	-0.278624542
1	-1.476531549	1.475366563	0.275806654
1	2.036021027	-2.037271320	1.678965776
1	-2.032512289	-2.033425099	-1.680138843
1	2.041452966	2.041750297	-1.678164574
1	-2.037370651	2.036360009	1.678494238
8	1.367045305	-1.369503636	-1.299598304
8	-1.371431630	-1.371402352	1.301930294
8	1.368082809	1.368253721	1.297907188
8	-1.369660359	1.366474549	-1.299948619
1	0.401581494	-1.507377876	-1.478424651
1	-0.407317393	-1.511626496	1.485022251
1	0.403604962	1.507529892	1.479860865
1	1.508965732	-0.406260312	-1.485096300
1	-1.506966142	0.400982470	-1.479013393
1	1.507391695	0.403822272	1.480052086
1	-1.511443662	-0.407346102	1.485401884
1	-0.406429932	1.508942842	-1.485098390

References

- [1] V. Medabalmi, N. Kaunr, and K. Ramanujam, *J. Electrochem. Soc.* **2017**, 164(1), A6147-A6153.
- [2] R. S. Nicholson, *Anal. Chem.* **1965**, 37, 1351
- [3] R. J. Klingler, J. K. Kochi, *J. Phys. Chem.* **1981**, 85, 1731.
- [4] Trivedi, D. R.; Fujiki, Y.; Fujita, N.; S. Shinkai, Sada, K. *Chem. Asian. J.* **2009**, 4, 254.
- [5] Parr, R. G.; Yang, W. *Density Functional Theory of Atoms and Molecules*; Oxford University Press: New York, 1989
- [6] Neese, F. *WIREs Comput. Mol. Sci.* **2018**, 8, 1.
- [7] Becke, A. D. *Phys. Rev. A* **1988**, 38, 3098.
- [8] Perdew, J. P. *Phys. Rev. B* **1986**, 33, 8822.
- [9] Grimme, S.; Antony, J.; Ehrlich, S.; Krieg, H. *J. Chem. Phys.* **2010**, 132, 154104.
- [10] Grimme, S.; Ehrlich, S.; Goerigk, L. *J. Comput. Chem.* **2011**, 32, 1456–1465
- [11] Weigend, F.; Ahlrichs, R. *Phys. Chem. Chem. Phys.* **2005**, 7, 3297–3305
- [12] Pettersen, E. F.; Goddard, T. D.; Huang, C. C.; Couch, G. S.; Greenblatt, D. M.; Meng, E. C.; Ferrin, T. E. *J. Comput. Chem.* **2004**, 25, 1605–1612.
- [13] Singh, V.; Kim, S.; Kang, J.; Byon, H. R. *Nano Res.* **2019**, 12, 1988-2001.